Nonlinear Damping in an Energy Harvesting Device

Luigi Simeone, Maryam Ghandchi Tehrani, Stephen Elliott and Mehdi Hendijanizadeh

l.simeone@soton.ac.uk

m.ghandchi-tehrani@soton.ac.uk

S.J.Elliott@soton.ac.uk

m.hendijanizadeh@soton.ac.uk

University of Southampton-Institute of Sound and Vibration Research

Abstract

Energy harvesting from ambient vibration has attracted significant attention in recent years. Some interesting applications include low-power wireless sensors, harvesting power from human motion and large-scale energy harvesters. In order to increase the *frequency range* of the excitation amplitude over which the vibration energy harvester operates, various nonlinear arrangements have been suggested, particularly using nonlinear springs [1-5]. In contrast, it has recently been shown that the *dynamic range* of a vibration energy harvester can be increased using a nonlinear damper [5]. Nonlinear damping, particularly stiction, can, however, also be an unwanted problem in practical power harvesters. However, this paper considers the effect of stiction, as Coulomb damping, on the performance of such a vibration power harvester.

A mechanical single degree-of-freedom nonlinear oscillator is considered, subjected to a harmonic base excitation. The relative displacement and the average harvested power are obtained for different sinusoidal base excitation amplitudes and frequencies, both analytically and numerically. The performance of the nonlinear harvester at different excitation levels is compared with a linear harvester, which has the same maximum relative displacement at resonance when driven at maximum amplitude. It is demonstrated that the nonlinear harvester can harvest much more energy, compared to the linear one, when driven below its amplitude threshold [5]. The effect of Coulomb damping, as a source of loss, is also investigated, for the harvesters with a linear damping and a cubic damping. It is shown that the Coulomb damping can reduce the amount of the harvested energy, particularly at low excitation amplitudes.

Keywords: energy harvesting, frequency range, friction, nonlinear damping

1 Introduction to nonlinear energy harvester

An inertial energy harvesting system is shown in Figure 1.

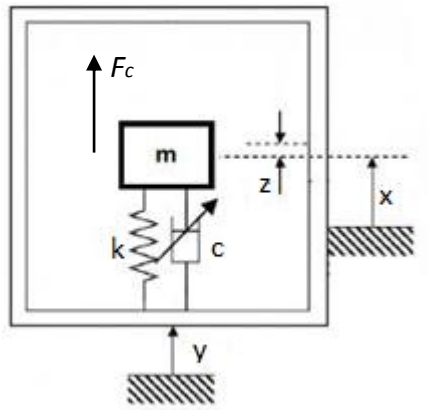

Figure 1: SDOF energy harvester, base excited with a nonlinear damper

It is composed by a suspended mass m, a stiffness k and a damping c and it is subjected to a base excitation y.

The damping force is nonlinear. A purely cubic viscous damping model ($f_d(t) = c_3 \dot{z}^3$) and a polynomial viscous damping model ($f_d(t) = c_1 \dot{z} + c_3 \dot{z}^3$) are compared each other and to an equivalent linear system. In particular, for the polynomial damping only the cubic term provides power harvested while the linear term is considered as a loss.

To represent the effect of friction, the Coulomb model was used and only the static friction was taken into account.

$$F_c = f_s \operatorname{sgn}(\dot{z}(t)) \tag{1}$$

The coefficient f_s is the static friction force.

The governing equation of motion for a polynomial viscous damping model is reported below:

$$m\ddot{z}(t) + c_1 \dot{z}(t) + c_3 \dot{z}^3(t) + f_s \operatorname{sgn}(\dot{z}(t)) + kz(t) = -m\ddot{y}(t) \tag{2}$$

The base excitation is supposed to be harmonic:

$$y(t) = Y \sin(\omega t - \varphi) \tag{3}$$

where Y is the input magnitude, ω is the frequency, and φ is the phase.

To approximate the response, the harmonic balance method was adopted. The assumption of this method is that the response is a harmonic function with the same frequency but a different phase and amplitude with respect to the input signal.

To apply this method, the sign function was decomposed in Fourier series [4]:

$$\operatorname{sgn}(\cos \omega t) = \frac{4}{\pi} \cos \omega t + \frac{4}{3\pi} \cos 3\omega t + \frac{4}{5\pi} \cos 5\omega t + ... \approx \frac{4}{\pi} \cos \omega t \tag{4}$$

As aforementioned, only the first harmonic was considered.
The relative transmissibility amplitude for a polynomial damping and a cubic damping is respectively:

$$\left|\frac{Z}{Y}\right| = \frac{m\omega^2}{\sqrt{\left(k - m\omega^2\right)^2 + \left(c_1\omega + \frac{3}{4}c_3\omega^3 Z^2 + \frac{4f_s}{\pi Z}\right)^2}} \qquad \left|\frac{Z}{Y}\right| = \frac{m\omega^2}{\sqrt{\left(k - m\omega^2\right)^2 + \left(\frac{3}{4}c_3\omega^3 Z^2 + \frac{4f_s}{\pi Z}\right)^2}} \tag{5}$$

In this case, it is assumed that, only the power absorbed by the cubic damper is available for harvesting:

$$P_{harvest} = \frac{1}{T}\int_0^T \left(c_3\dot{z}^3\right)\dot{z}dt = \frac{3}{8}c_3\omega^4 Z^4 \tag{6}$$

Whereas, power dissipated by Coulomb damping, which is not available and is lost, can be computed considering the power dissipated in a period:

$$P_{loss} = \frac{1}{T}\int_0^T \left(f_s \operatorname{sgn}(\dot{z})\right)\dot{z}dt = \frac{4f_s Z\omega}{\pi} \tag{7}$$

To sum up, in the Table 1 and Table 2, are reported both the power harvested and the loss power for two systems (without and with Coulomb friction).

Table 1: Harvested and loss power for linear, cubic and polynomial damping models - No Coulomb friction

Model	Harvested	Loss
Linear	$P_{ave} = \frac{1}{2}c_1\omega^2 Z^2$	No loss
Cubic	$P_{ave} = \frac{3}{8}c_3\omega^4 Z^4$	No loss
Polynomial	$P_{ave} = \frac{3}{8}c_3\omega^4 Z^4$	$P_{loss} = \frac{1}{2}c_1\omega^2 Z^2$

Table 2: Harvested and loss power for linear, cubic and polynomial damping models – With Coulomb friction

Model	Harvested	Loss
Linear + Coulomb	$P_{ave} = \frac{1}{2}c_1\omega^2 Z^2$	$P_{loss} = \frac{4f_s Z\omega}{\pi}$
Cubic + Coulomb	$P_{ave} = \frac{3}{8}c_3\omega^4 Z^4$	$P_{loss} = \frac{4f_s Z\omega}{\pi}$
Polynomial + Coulomb	$P_{ave} = \frac{3}{8}c_3\omega^4 Z^4$	$P_{loss} = \frac{1}{2}c_1\omega^2 Z^2 + \frac{4f_s Z\omega}{\pi}$

2 Simulated results

The simulation parameters for the single degree of freedom energy harvester are:

$m = 1kg,\ k = 4\pi \frac{N}{m},\ Y_{\max} = 0.246m,\ Z_{\max} = 1m,\ f_s = 1N,\ c_{1eq} = 1.55\frac{Ns}{m},\ \omega_n = 2pi\frac{rad}{s}.$

The nonlinear systems were compared with an equivalent linear system.
The equivalent linear damping coefficient was computed at maximum displacement amplitude when the system was driven at resonance. In Table 3 and
Table **4**, the damping coefficients for the nonlinear and the equivalent linear system are reported.

Table 3: Damping coefficients - No friction

Model	C_1	C_3
Linear	1.55	0
Cubic	0	0.052
Polynomial	0.77	0.0263

Table 4: Damping coefficients - With friction

Model	C_1	C_3	f_s
Lin + Coulomb	1.347	0	1
Cub + Coulomb	0	0.046	1
Polyn + Coulomb	0.77	0.0195	1

For example, for a purely cubic model:

$$c_{1eq} = \frac{3}{4}c_3\omega_n^2 Z_{\max}^2 \qquad (8)$$

The six systems, shown in Table **1**Table **2** were forced to have the same output amplitude at resonance when the input amplitude is equal to its maximum operational limit, for a fixed value of f_s.
The comparison between nonlinear models was carried out both analytically and numerically.
From the analytical point of view the harmonic balancing method was applied.
The assumption of this method is that the response of the system is a harmonic function with the same frequency but a different phase and amplitude with respect to the input signal.
The Eq.2 is solved numerically using the ode45 algorithm, substituting the sign function with the hyperbolic tangent function. This is due to the fact that the sign function makes the problem too stiff to be easily computed.
In the following a system affected by Coulomb friction is compared to another one with no friction.
This comparison is carried out both in term of relative transmissibility amplitude and average power absorbed.

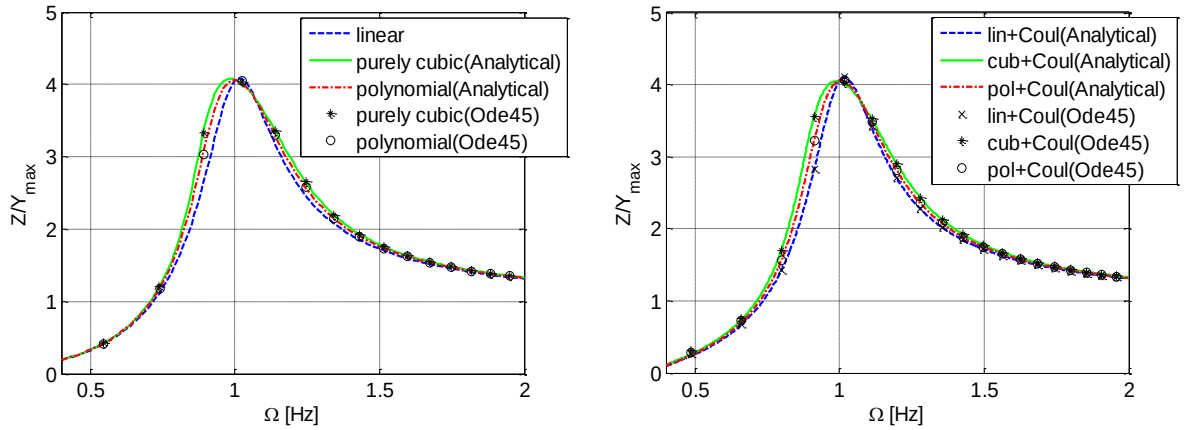

Figure 2: Relative transmissibility for a system driven at maximum amplitude with no Coulomb friction (a) and affected by Coulomb friction (b)

On the x-axis the non-dimentional frequency is reported $\Omega = \frac{\omega}{\omega_n}$.

In Figure 2, it is shown as the systems have the same response at resonance when $Y = Y_{\max}$. When a polynomial damping is taken into account only the cubic term is considered as power harvested.
As shown in Figure 3, the polynomial damping allows us to store less energy than the linear and the cubic damping. This is due to the fact that the linear term is loss power.

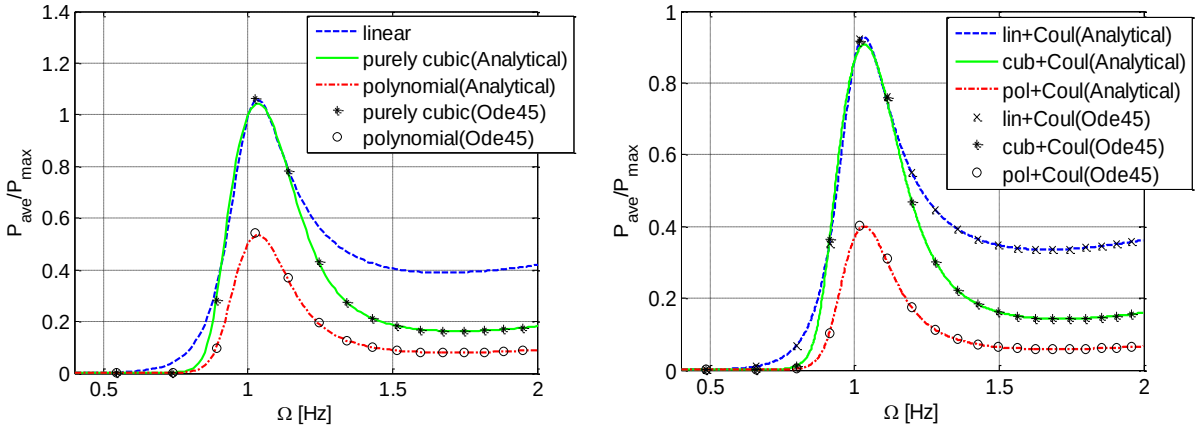

Figure 3: Average power for a system driven at maximum amplitude with no Coulomb friction (a) and affected by Coulomb friction (b)

Therefore, in a system affected by Coulomb friction the polynomial damping has two sources of loss: the linear term and the stiction.
As known, nonlinear systems are strongly influenced by a change in input amplitude.
This effect can be used to increase the range of performance if the system is driven off the maximum amplitude.
This phenomenon is evident in the level curves.
The level curves represent the relative transmissibility amplitude and the average power, at resonance, as a function of input amplitude base displacement.

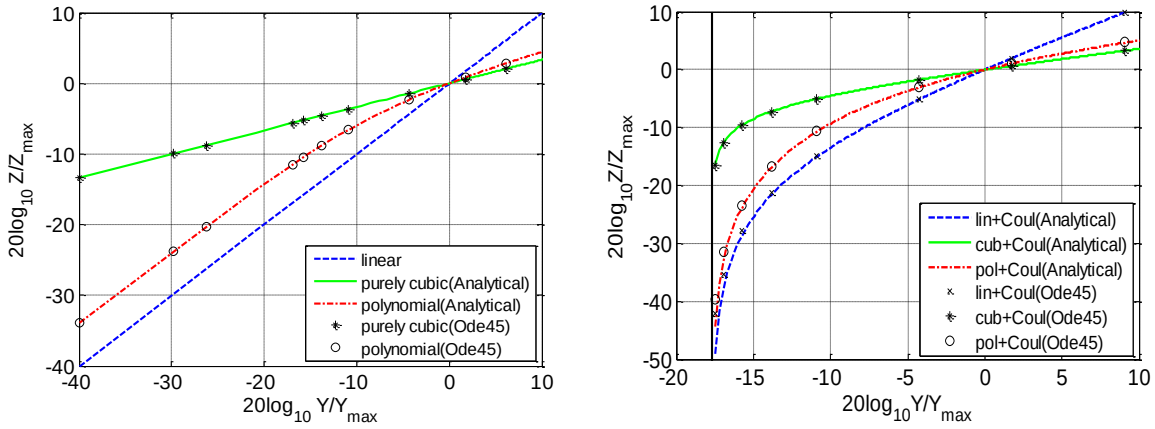

Figure 4: Level curves – Relative transmissibility for a system with no Coulomb friction (a) and affected by Coulomb friction (b)

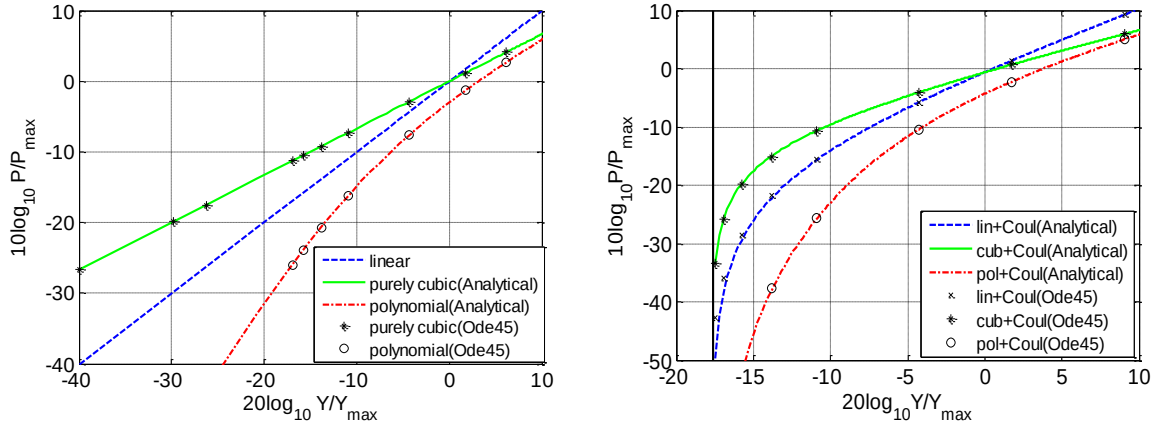

Figure 5: Level curves – Average power for a system with no Coulomb friction (a) and affected by Coulomb friction (b)

Some observations can be inferred from Figure 4 and Figure **5**.
Introducing Coulomb friction, a global reduction in terms of average power is evident if compared to a system with no friction.
As reported, both numerically and analytically, the model that allows us to harvest more energy is the purely cubic damper for both a system affected by Coulomb friction and no friction. The less efficient model is the polynomial damping.
In Figure 4b and Figure 5b, there exists a lower limit on input amplitude that represents a threshold below that the output amplitude displacement, *Z*, starts to be negative. This happens for different coefficients c_1, c_3, f_s.
As aforementioned, in Figure 5, the polynomial model allows us to harvest much less energy than the linear and the cubic system. In particular, in the linear plus Coulomb and cubic plus Coulomb models the only loss is the friction while in the polynomial plus Coulomb model, the system is affected by two dissipative forces (Figure 5(b)), the linear viscous damping and the friction.

3 Experimental test rig

A test rig is built to verify the correctness of simulated results.
It is a rotational energy harvester shown in Figure 6. It is composed by a seismic mass m, a ball screw (utilized to convert linear motion of the mass to a rotational motion to drive a rotary generator), and two springs.

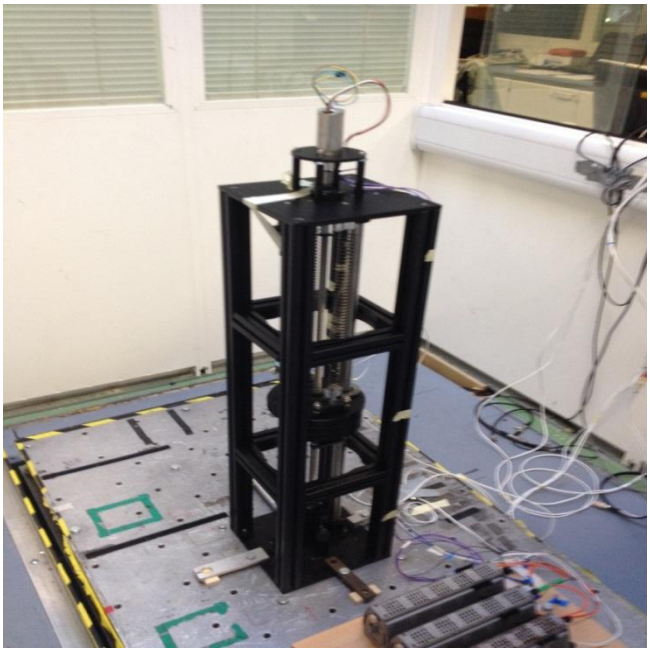

Figure 6: Experimental test rig

From a practical point of view two different experimental conditions were taken into account:

- Open circuit: in which the only contribution to the damping is due to mechanical effects;
- Load circuit: in which the contribution to the damping is due to both mechanical and electrical effects.

The non-conservative forces were modelled as Coulomb friction and linear viscous damping.
In particular, the viscous damping coefficient is influenced by both the mechanical and electrical circuit [6-7].
The harvester was based excited by a sinusoidal force.

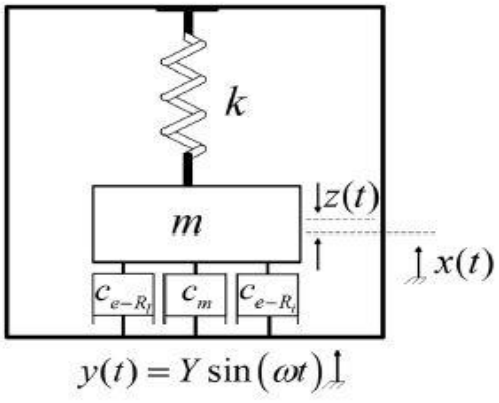

Figure 7 Sketch representation of test rig

The equation of motion for the harvester, sketched in Figure 7, can be written as follows:

$$M\ddot{z}(t)+\left(\frac{2\pi}{l}\right)^2\left(c_m + c_{e-Rl} + c_{e-Ri}\right)\dot{z}(t)+ f_s\,\mathrm{sgn}\left(\dot{z}(t)\right)+ kz(t) = -m\ddot{y}(t) \qquad (9)$$

The parameters are listed below:

$$M = m + \left(\frac{2\pi}{l}\right)^2 \left(J_{b-s} + J_g + J_c\right) = 12.84kg \tag{10}$$

In particular, $m = 8kg$ is the seismic mass, the term $\left(\frac{2\pi}{l}\right)^2 \left(J_{b-s} + J_g + J_c\right)$ is the reflected mass of the ball screw, generator, and the coupling shaft between ball screw and the generator, and $l = 0.02m$ is the ball screw lead [6-7].

$$c_g = \left(\frac{2\pi}{l}\right)^2 \left(c_m + c_{e-Rl} + c_{e-Ri}\right) = c_m^{'} + \left(\frac{2\pi}{l}\right)^2 \frac{\alpha K_t^2}{R_i + R_l} \tag{11}$$

The rotational mechanical viscous damping $c_m^{'}$ was computed.

The coefficient α is due to the fact that the electrical part is a three-phase system ($\alpha = 3$):
If:

$K_t = 0.0232 \frac{Nm}{A}$ transduction coefficient

$R_i = 0.1ohm$ electrical internal resistance of generator

$R_l = 0.5ohm$ electrical load resistance

$$\left(\frac{2\pi}{l}\right)^2 \frac{\alpha K_t^2}{R_i + R_l} = 255 \frac{Ns}{m} \tag{12}$$

The power harvested is only due to the electrical load resistance, thus:

$$P_{ave} = \frac{1}{2\pi} \int_0^{2\pi} \left(\frac{2\pi}{l}\right)^2 c_{e-Rl} \dot{z}^2 dt = \frac{1}{2} \left(\frac{2\pi}{l}\right)^2 \frac{3R_l K_t^2}{\left(R_l + R_i\right)^2} \omega^2 Z^2 \tag{13}$$

The stiffness is $k = 250 \frac{N}{m}$.

The friction coefficient f_s has to be defined yet.

4 Estimation of friction and rotational mechanical viscous damping coefficients

In the Eq.9, the only unknown parameters are f_s, $c_m^{'}$.

Firstly the static friction coefficient was computed.

It was estimated experimentally by moving the suspended mass upwards and downwards from the equilibrium position. After releasing, the positions are measured in static conditions (x_1, x_2).

The coefficient is computed by solving the two equilibrium equations:

$$f_s + kx_1 = mg \tag{14}$$

$$kx_2 = f_s + mg \tag{15}$$

$$\Rightarrow f_s = 8.37N$$

The mechanical damping is not controllable. The goal would be to tune R_l so that the difference between the electrical and the mechanical contributions can be maximized.

The parameter $c_m^{'} = \left(\frac{2\pi}{l}\right)^2 c_m$ was estimated using the experimental curve in open circuit to avoid uncertainties due to the electrical coupling. Analyses were carried out to obtain the optimized rotational mechanical damping for the best fit.

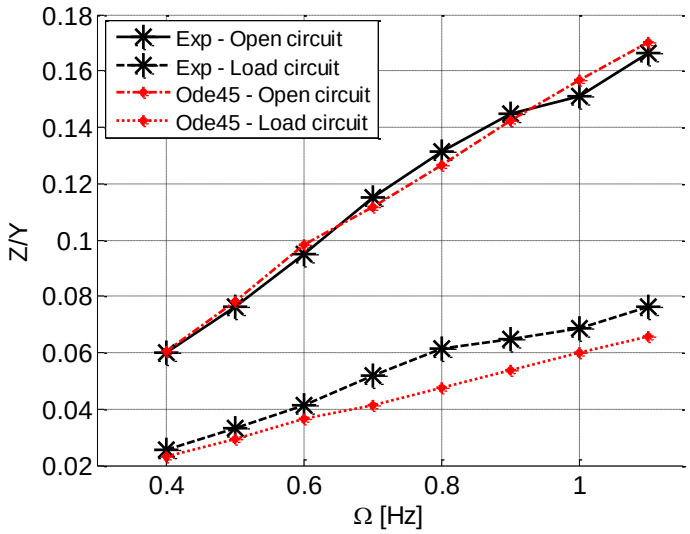

Figure 8: Transmissibility as a function of frequency - numerical fitting for open and load circuit

The value of $c_m^{'}$ was obtained by changing iteratively its value, until the best fit is obtained between the dash dot red line and the solid black line in Figure 8.

The resonant frequency is $0.7Hz$.

After computing $c_m^{'}$, adding electrical damping, Eq.12, the global rotational viscous damping coefficient was found.

$$c_m^{'} = 170\frac{Ns}{m} \qquad c_g = 425\frac{Ns}{m} \tag{16}$$

In Figure 8, it is shown that the system is overdamped for both open and load circuit, so no amplitude peak is evident in fact:

$$\zeta_{load} = \frac{c}{c_{cr}} = \frac{\left(\frac{2\pi}{l}\right)^2 \left(c_m + c_{e-Rl} + c_{e-Ri}\right)}{2M\omega_n} = 3.76 \qquad \zeta_{open} = \frac{\left(\frac{2\pi}{l}\right) c_m}{2M\omega_n} = 1.5 \tag{17}$$

The storable power is proportional to the n-power of the relative displacement Z, therefore, an overdamped system can supply less power than an underdamped system in the same conditions.

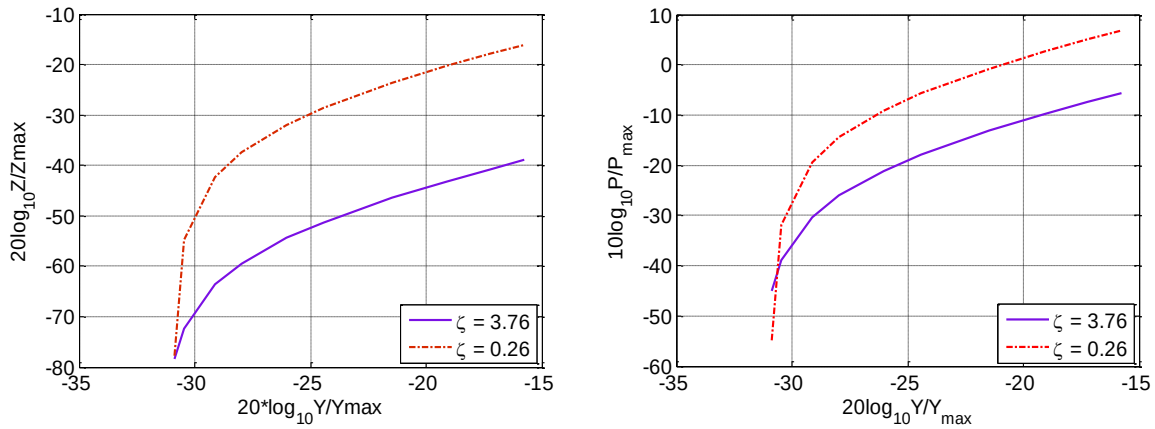

Figure 9: Effect of input amplitude on relative displacement (a) and power harvested (b) for underdamped and overdamped system (Load circuit) – Simulated results

In Figure 9 it is evident that the power harvested (and the relative transmissibility) decrease consistently passing from an underdamped (dash dot red line) to an overdamped (solid blue line) system.

An important aspect to evaluate is the influence of the input amplitude.

The experimental level curves in open and load circuit were obtained and compared to the numerical results.

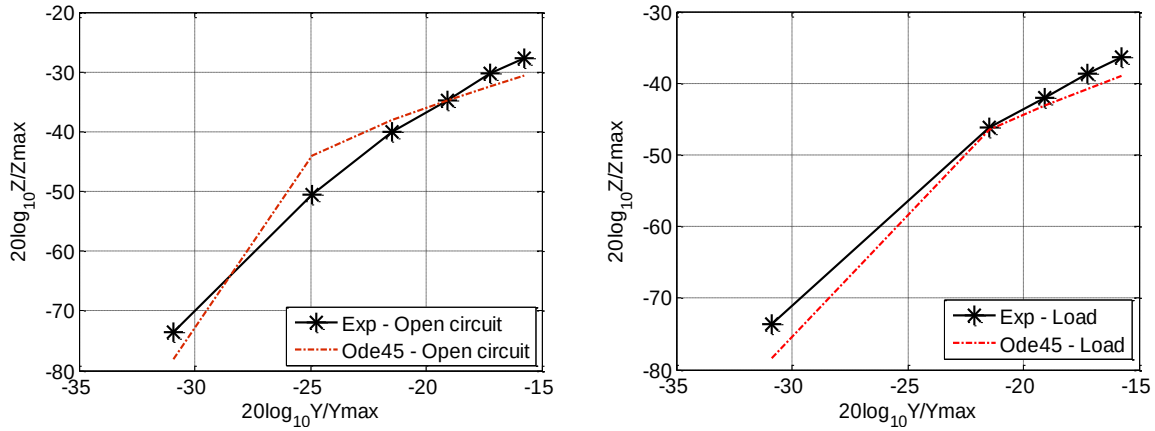

Figure 10: Relative displacement as a function of input amplitude - Open (a) and load circuit (b)

Figure 10 shows a good match between numerical and experimental results in both conditions.

To evaluate the influence of another source of nonlinearity, a purely cubic damping model was added to the actual system (Figure 11).

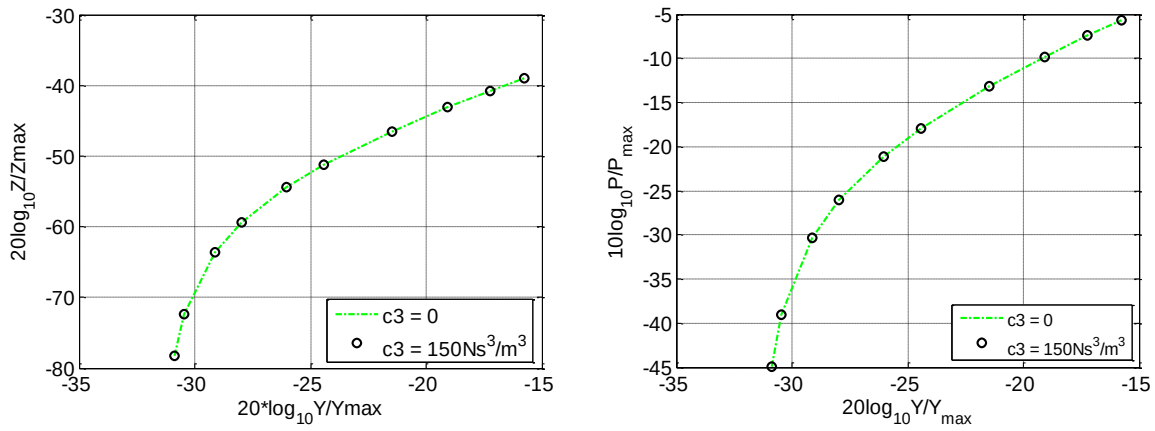

Figure 11: Relative displacement (a) and power harvested (b) as a function of Y (Load circuit) - Simulated results

As already said, only the electrical linear viscous damping (due to the electrical load resistance) provides energy harvested.

Unlike an underdamped system, the effect of the cubic damping in an overdamped system is almost negligible. The dynamics are controlled by the linear viscous damping and adding a cubic damping the amount of the harvested power cannot be increased.

In particular, to appreciate the effect of the cubic damping, the coefficient c_3 should be increased of other orders of magnitude.

5 Conclusion

This paper was focused on the effect of nonlinear damping models in a *SDOF* energy harvester.

A purely cubic and a polynomial damping forces were considered in a system affected by Coulomb friction, and compared with an equivalent linear system.

To compare the performance of these different models in terms of relative transmissibility and average power, an equivalent linear system was found. Consequently these systems were forced to have the same response at resonance when driven to work at maximum level of input excitation.

The friction is always considered as a loss.

Observing Figure 4 and Figure 5, if a Coulomb friction is introduced a global reduction in terms of harvested power is evident.

As reported, cubic model is the most efficient. It allows us to enlarge the range of performance much more than a linear and a polynomial model.

However c_1, c_3, f_s are fixed, there exists a lower limit on input amplitude Y that represents a threshold below that the output amplitude displacement Z starts to be negative.

The second part of this paper was dedicated to the test rig.

A rotational energy harvester is considered and two different experimental conditions were taken into account:

- Open circuit: in which the only contribution to the damping is due to mechanical effects;
- Load circuit: in which the contribution to the damping is due to both mechanical and electrical effects;

The only parameters unknown were the Coulomb coefficient f_s and the rotational viscous damping coefficient $c_m^{'}$.

First f_s was measured. The static friction was obtained experimentally from the static equilibrium positions.
Afterwords, the rotational mechanical viscous damping was found fitting the experimental data in open circuit.
As shown in Figure 8, the test rig presents an overdamped behaviour both in open and in load circuit.
The transmissibility does not have any peak at resonance and, therefore, it is not possible to use the high output amplitude to harvest more power.
Another consequence of an overdamped behaviour is that the system is less sensitive to other sources of nonlinearity as, for instance, a purely cubic damping model.

Acknowledgement

The authors acknowledge the support provided by the EPSRC from grants EP/K005456/1, EP/K003836/1 and "Engineering Nonlinearity".

References

[1] B. P. Mann and N. Sims, Using nonlinearity to improve the performance of vibration-based energy harvesting devices, 7th European Conference on Structural Dynamics, Southampton July 2008.

[2] R. Ramlan, M.J. Brennan, B.R. Mace and I. Kovacic, Potential benefits of a non-linear stiffness in an energy harvesting device, Nonlinear Dynamics, 59 (2010) 545-558.

[3] B. P. Mann and N. D. Sims, Energy harvesting from the nonlinear oscillations of magnetic levitation, Journal of Sound and Vibration, 319(1-2),(2009),515–530.

[4] P.L. Green, K. Worden, K. Atallah, and N.D. Sims, The effect of duffing-type non-linearities and coulomb damping on the response of an energy harvester to random excitations, Journal of Intelligent Material Systems and Structures, (2012), doi: 10.1177/1045389X12446520.

[5] M. Ghandchi Tehrani and S. J. Elliott, Extending the dynamic range of an energy harvester using nonlinear damping, Journal of Sound and Vibration, **333** (2014) 623-629.

[6] M. Hendijanizadeh, M. M. Torbati, S. M. Sharkh, Constrained Design Optimization of Vibration Energy Harvesting Devices, Journal of Vibration and Acoustics, APRIL 2014, Vol. 136 / 021001-1.

[7] M. Hendijanizadeh, S. M. Sharkh, S. J. Elliott, M. M. Torbati, Output power and efficiency of electromagnetic energy harvesting systems with constrained range of motion, Smart Materials and Structures 22 (2013) 125009 (10pp).